PHYSICAL REVIEW B VOLUME 40, NUMBER 7 1 SEPTEMBER 1989

Anomalous incommensurability and local ordered states at first-order phase transitions

K. Fuchizaki
Faculty of Engineering Science, Osaka University, Toyonaka-shi, Osaka 560, Japan

Y. Yamada
Institute for Solid State Physics, The University of Tokyo, 7-22-1, Roppongi, Minato-ku, Tokyo 106, Japan
(Received 16 March 1989)

Anomalous incommensurability in the diffraction pattern observed as a precursor of various first-order phase transitions is discussed on a phenomenological basis. The anomaly is characterized by the incommensurability which is dependent on the reference Brillouin zone. Starting from a general free-energy functional describing a first-order phase transition, we obtain spatially modulated solutions of the order parameter as well as of the strain field, which we call "embryonic fluctuation." Diffraction profiles are calculated for the system with random distribution of embryonic fluctuations, which turned out to reproduce the observed anomalous incommensurability.

I. INTRODUCTION

In recent years, pretransitional phenomena associated with first-order structural phase transitions have attracted considerable attention, particularly in connection with martensitic transformations in metals. The principal features of interest seem to be related to the incomplete softening of particular phonon modes.

When the transition is caused by complete phonon softening, the transition will be of second order, and it will be preceded by the critical fluctuations of the order parameter whose nature is well understood based on the theories of critical phenomena at second-order phase transitions. The incompleteness of the lattice instability leads to the first-order nature of the phase transition. Nevertheless, various kinds of pretransitional phenomena[1-5] around martensitic transformation such as "tweed pattern" formation observed with electron microscopy, anomalies in transport properties, anomalous increase of internal friction, the appearance of the central peak detected by neutron scattering, anomalous x-ray scattering, etc. have been reported. In particular, the x-ray scattering at pretransitional states in the alloy TiNi was reported to show remarkable peculiarity as summarized in the following paragraph.

The alloy TiNi, a well-known shape-memory alloy, undergoes a phase transition with decreasing temperature from a β_1 structure to a martensite phase through softening of TA phonon mode with $\mathbf{q}=\frac{1}{3}[110]$. Salamon[2] first reported that there appears an intermediate state where the $\mathbf{q}$ values of the superlattice reflections are incommensurate before they "lock" into the exact commensurate value of $\frac{1}{3}$ in the low-temperature phase. In a high-resolution x-ray study Shapiro *et al.*[4] found anomalous behavior associated with the incommensurability of the satellite peaks: Note only are they incommensurate in position, but also the incommensurability $\Delta\mathbf{q}$ changes from Brillouin zone to Brillouin zone. Moreover, the pair of peaks within a Brillouin zone does not satisfy the center of symmetry around the Brillouin-zone center, as it usually does, but only maintains symmetry around the origin of the reciprocal lattice. These unusual symmetry properties of $\Delta\mathbf{q}$ definitely rule out the ordinary incommensurate structure with charge-density waves (CDW's) or lattice-distortion waves (LDW's), in which case satellites should satisfy the center of symmetry around each Brillouin-zone center as well as the translational symmetry with respect to translation of Brillouin zones.

Salamon *et al.*[6] first pointed out a very interesting feature on this anomalous incommensurability of the satellites in TiNi: As is illustrated in Fig. 1, the observed diffraction pattern can be systematically reproduced if we assume that *only* satellite peaks have shifted to the positions expected in the rhombohedral martensite phase, while the Bragg peaks still maintain the original cubic positions. They referred to this peculiar reciprocal lattice as the "ghost lattice."

Yamada *et al.*[7-9] constructed a possible microscopic model to explain the physical origin of the ghost lattice. The basic idea of their model is that (i) the bcc matrix has a particular elastic property represented by a dip in TA phonon mode or the presence of the soft mode (ii) in the pretransitional state many embryos or locally transformed microregion of low-temperature structures are distributed in the matrix. They set up model systems of 1D and 2D lattices of atoms whose phonon dispersion has soft phonon modes. The displacement field is then calculated when the lattice is strained by a specific type of Kanzaki force[10] which stands for the existence of embryos. They showed that the diffraction pattern of this spontaneously strained lattice reproduces the characteristics of the ghost lattice.

Although their treatment elucidated a possible origin of anomalous incommensurability of the ghost lattice, the discussion based on such a specific model left the point of generality and overall applicability of the idea unclear. In the present paper, we discuss the same problem from a different standpoint.

We start from a general expression of phenomenologi-

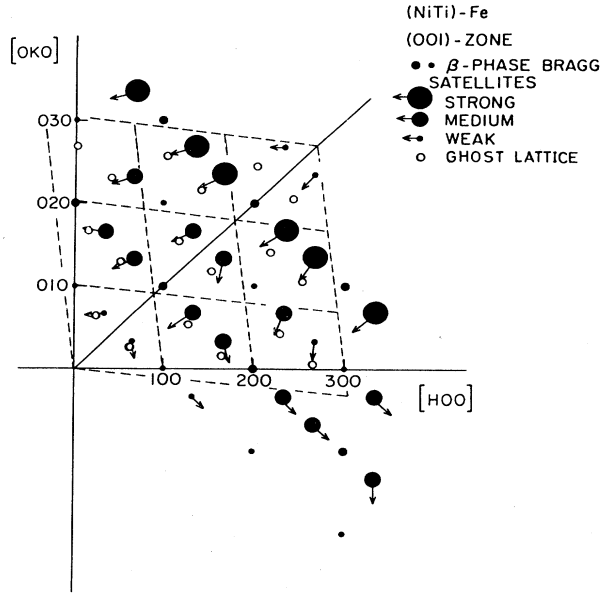

FIG. 1. Relation between satellite reflections observed by Shapiro *et al.* (Ref. 4) and the rhombohedral ghost lattice. The arrows represent the directions of displacements from the exact commensurate cubic positions, whose relative magnitudes are expressed by the length of the arrows. Note that the satellites, with few exceptions, shift generally toward rhombohedral satellite positions (shown by the open circles) while the fundamental Bragg reflections are centered on cubic reciprocal lattice points.

cal free energy which describes a first-order phase transition. The characteristic feature of the free energy relevant to first-order phase transition is depicted in Fig. 2. We assume that in the temperature range of $T \gtrsim T_c$, there are chances that the order parameter ξ is *locally* (and temporally) locked in the metastable state with $\xi = \bar{\xi}$. Since $\bar{\xi}$ gives the order parameter in the low-temperature phase, the locally locked-in state with $\xi = \bar{\xi}$ may be called an "embryonic fluctuation." The overall spatial variation

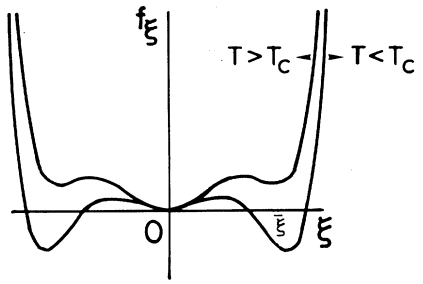

FIG. 2. Schematic illustration of a potential function f_ξ describing the first-order phase transition. The abscissa represents the order parameter ξ. Note that the states corresponding to $\xi = \pm\bar{\xi}$ (at which the potential have local minima) are energetically degenerate, which is essential to the low-temperature ($T < T_c$) structure with two variants of ordered phase.

of the order parameter $\xi(\mathbf{r})$ is obtained by the standard procedure to minimize the free-energy functional under such a boundary condition that embryonic fluctuations are excited randomly within the system. As the displacement field is given in terms of $\xi(\mathbf{r})$, we can calculate the diffraction pattern in the precursor state $T \gtrsim T_c$. This procedure gives an alternative way to discuss the observed ghost lattice behavior.

Since these arguments are based on a purely phenomenological standpoint, the results are quite general and give a comprehensive perspective view of the origin of the ghost lattice and its relation to first-order phase-transition phenomena.

In the next section, a free-energy functional which describes first-order phase transition including the coupling between the order parameter and a macroscopic strain is established. Spatial variations of the order parameter $\xi(\mathbf{r})$ as well are of the strain $e(\mathbf{r})$ are obtained under the boundary condition suitable for a state of embryonic fluctuation. The results are utilized to calculate the diffraction pattern in Sec. III, which eventually reproduces the characteristics of the ghost lattice. In Sec. IV we will discuss the obtained results in connection with the recent experimental results.

II. FREE ENERGY AND EMBRYONIC FLUCTUATION

The order parameter associated with a displacive phase transition is the amplitude of the phonon mode which freezes in the ordered phase. That is, the displacement in the low-temperature (ordered) phase at the jth site is given by

$$\mathbf{u}(\mathbf{r}_j) = \xi \mathbf{e}(\mathbf{q}_0)\exp(i\mathbf{q}\cdot\mathbf{r}_j) + \text{c.c.} \ , \tag{1}$$

where $\mathbf{q}_0$ and $\mathbf{e}(\mathbf{q}_0)$ denote the wave vector and the polarization vector of the freezing (soft) mode, respectively. For simplicity, let us assume that $\mathbf{q}_0$ is at the zone boundary along the direction of one of the principal axes $\mathbf{a}$ of the crystal;

$$\mathbf{q}_0 = \tfrac{1}{2}\mathbf{a}^* \quad (|\mathbf{a}^*| = 2\pi/a) \tag{2}$$

and $\mathbf{e}(\mathbf{q}_0)$ is perpendicular to $\mathbf{a}^*$ (transverse mode). That is, the ordered structure is of the antiferro type.

Since we are considering that the phase transition is of first order, the free-energy density expanded with respect to $\xi(\mathbf{r})$ should be given by

$$\tilde{f}_\xi(\xi) = \frac{\kappa_1}{2}\left[\frac{\partial \xi}{\partial x}\right]^2 + f_\xi(\xi) \ , \tag{3}$$

$$f_\xi(\xi) = \frac{\alpha}{2}\xi^2 + \frac{b}{4}\xi^4 + \frac{c}{6}\xi^6, \quad \alpha = \alpha_0(T - T_0)$$

$$\kappa_1 > 0, \quad \alpha_0 > 0, \quad b < 0, \quad c > 0 \ . \tag{4}$$

The first term in Eq. (3) takes care of the energy due to spatial modulation of the order parameter. Equation (4) is the well-known functional form to describe the first-order phase transition which satisfies the symmetry property $f_\xi(-\xi) = f_\xi(\xi)$.[11] This twofold symmetry is essen-

tial to the low-temperature structure with two variants of ordered phase.

The structural transformation in solids is usually accompanied by a volume and/or shape change. In order to include this effect, strain energy contribution to the free energy should be taken into account. The strain free-energy density f_e associated with the longitudinal strain component e_{11} is given by

$$\tilde{f}_e(e_{11})=\frac{\kappa_2}{2}\left[\frac{\partial e_{11}}{\partial x}\right]^2+f_e(e_{11}) , \tag{5}$$

$$f_e(e_{11})=\frac{\chi}{2}e_{11}^2, \quad \kappa_2>0, \quad \chi>0 \tag{6}$$

in which the energy increase due to the spatial variation of e_{11} is given by the first term in Eq. (5).

We assume that there exists strong coupling between the order parameter ξ and the longitudinal strain component e_{11}. Taking into account the translational invariance of each energy term, the lowest-order coupling energy is given by

$$f_c(\xi,e_{11})=\lambda e_{11}\xi^2 , \tag{7}$$

where λ is a coupling coefficient.

Thus, combining all energy terms, the total energy functional is expressed by

$$\begin{aligned}F[\xi,e_{11}]&=\int d\mathbf{r}(\tilde{f}_\xi+\tilde{f}_e+f_c) ,\\ &=\int d\mathbf{r}\left[\frac{\kappa_1}{2}\left[\frac{\partial\xi}{\partial x}\right]^2+\frac{\kappa_2}{2}\left[\frac{\partial e_{11}}{\partial x}\right]^2\right.\\ &\qquad\left.+\hat{f}(\xi,e_{11})\right] ,\end{aligned} \tag{8}$$

$$\hat{f}(\xi,e_{11})=f_\xi(\xi)+f_e(e_{11})+f_c(\xi,e_{11}) , \tag{9}$$

where the potential function $\hat{f}(\xi,e_{11})$ represents a homogeneous part of the free energy.

The feature of the transition of the system is most easily understood by drawing the potential surface within two-dimensional $(\xi-e_{11})$ space at various temperatures. We have chosen the coefficients in Eq. (9) appropriately such that $b=-140$, $c=4900$, $\chi=1$, and $\lambda=-1$ and have plotted the potential surface in Fig. 3(a).

For later convenience, let us divide the temperature region into the following subregions depending on the characteristic of the potential function.

(I) $T_1<T$; potential has single minimum at $\xi=(\xi,e_{11})=0$, $T_1=T_0+(\beta^2/4\alpha_0 c)$; (II) $T_c<T<T_1$, triple minima at $\xi=0$, and at $\xi=\pm(\bar{\xi},\bar{e}_{11})=\pm\bar{\xi}$; the latter two are energetically degenerate $[\hat{f}(0)<\hat{f}(\pm\bar{\xi})]$; $T_c=T_0+(3\beta^2/16\alpha_0 c)$; (III) $T_0<T<T_c$; triple minima at the same positions as those in (II), $[\hat{f}(0)>\hat{f}(\pm\bar{\xi})]$; (IV) $T<T_0$, double minima at $\xi=\pm\bar{\xi}$.

As is seen in Fig. 3(a), at dimensionless temperature $\tau\equiv(T-T_c)/(T_c-T_0)=0.3217$ ($\lesssim\tau_1=0.3333$), a relatively well-defined minimum is at $(\xi,e_{11})=(0,0)$. As τ is decreased there appears a minimum at $(\xi,e_{11})=(\bar{\xi},\bar{e}_{11})$ in addition to the minimum at the origin. The former is metastable when $\tau\geq\tau_c=0$, but becomes the absolute minimum for $\tau<\tau_c$. The uniform ordered phase which is characterized by spatially uniform $\bar{\xi}$ and $\bar{e}_{11}$ with

$$\bar{\xi}=\frac{\beta+(\beta^2-4\alpha c)^{1/2}}{2c}, \quad \beta=|b|+\frac{2\lambda^2}{\chi} \tag{10}$$

and

$$\bar{e}_{11}=-\frac{\lambda}{\chi}\bar{\xi}^2 , \tag{11}$$

is stabilized below the transition temperature.

We are particularly interested in the temperature region of $\tau_c<\tau<\tau_1$ [region (II)], because this region just corresponds to the precursor state. In this temperature regime, the stable state is, of course, given by $(\xi,e_{11})=(0,0)$. However, there may be a finite possibility that the system *locally* surmounts the potential barrier and is locked into the state $(\bar{\xi},\bar{e}_{11})$ simply by thermal fluctuation. This locally ordered state should fluctuate back to the stable state (0,0) within finite lifetime. We may expect the lifetime would be substantially longer than the period of lattice vibration. That is, the local ordered state (embryonic fluctuation) is quasistatic in the scale of phonon frequency.

Let us consider that an embryo is static and is sitting at a particular position $x=x_0$, and we investigate on the spatial variation of the order parameter $\xi(x)$ and the strain $e_{11}(x)$ under the particular boundary condition appropriate for the existence of the embryo:

$$\begin{aligned}&\xi=\bar{\xi} \ \text{ at } x=x_0, \ \ \xi\to 0 \ \text{ as } x\to\pm\infty ,\\ &e_{11}=\bar{e}_{11} \ \text{ at } x=x_0, \ \ e_{11}\to 0 \ \text{ as } x\to\pm\infty .\end{aligned} \tag{12}$$

We solve the following coupled Euler equations:

$$\begin{aligned}&-\kappa_1\frac{\partial^2\xi}{\partial x^2}+\frac{\partial\hat{f}}{\partial\xi}=0 ,\\ &-\kappa_2\frac{\partial^2 e_{11}}{\partial x^2}+\frac{\partial\hat{f}}{\partial e_{11}}=0\end{aligned} \tag{13}$$

under the above boundary condition. From Eq. (13), the first integral is readily obtained as

$$\left[\frac{\kappa_1}{2}\left[\frac{d\xi}{dx}\right]^2+\frac{\kappa_2}{2}\left[\frac{de_{11}}{dx}\right]^2\right]-\hat{f}(\xi,e_{11})=U_0 , \tag{14}$$

where U_0 is an integral constant.

When $\kappa_2=0$, Eq. (14) can be analytically solved for all temperature regions with appropriate boundary conditions. To get a feeling for the discussion below, it is worthwhile looking at a situation with $\kappa_2=0$. In region (II), the second boundary condition in Eq. (12) requires $U_0=0$. Equation (14) then becomes

$$\pm\left[\frac{\alpha}{\kappa_1}\right]^{1/2}dx=\frac{\frac{1}{2}d(\xi^2)}{\xi^2\left[1-\frac{\beta}{2\alpha}\xi^2+\frac{c}{3\alpha}\xi^4\right]^{1/2}} . \tag{15}$$

This can be easily solved to give

$$\xi(x)=\frac{2\gamma e^{\sqrt{\alpha/\kappa_1}(x-x_0)}}{\left\{\left[2\left[\frac{c}{3\alpha}\right]^{1/2}-\frac{\beta}{2\alpha}\right]\gamma^4 e^{4\sqrt{\alpha/\kappa_1}(x-x_0)}+\frac{\beta}{\alpha}\gamma^2 e^{2\sqrt{\alpha/\kappa_1}(x-x_0)}-\left[2\left[\frac{c}{3\alpha}\right]^{1/2}+\frac{\beta}{2\alpha}\right]\right\}^{1/2}}, \tag{16}$$

where the constant γ is determined by the first boundary condition in Eq. (12) as

$$\gamma^2=\frac{-\left[\frac{\beta}{2\alpha}\bar{\xi}^2-2\right]+2\left[\frac{c}{3\alpha}\bar{\xi}^4-\frac{\beta}{2\alpha}\bar{\xi}^2+1\right]^{1/2}}{\left[2\left[\frac{c}{3\alpha}\right]^{1/2}-\frac{\beta}{2\alpha}\right]\bar{\xi}^2}. \tag{17}$$

The solution (16) just above τ_c ($\tau=0.0003$) is shown in Fig. 4(a). From Eq. (13), $e_{11}(x)$ is given in terms of $\xi(x)$ as

$$e_{11}(x)=-\frac{\lambda}{\chi}\xi^2(x). \tag{18}$$

As τ approaches to τ_c, the spatial variations of $\xi(x)$ become kinklike, and eventually at $\tau=\tau_c$, $\xi(x)$ represents a

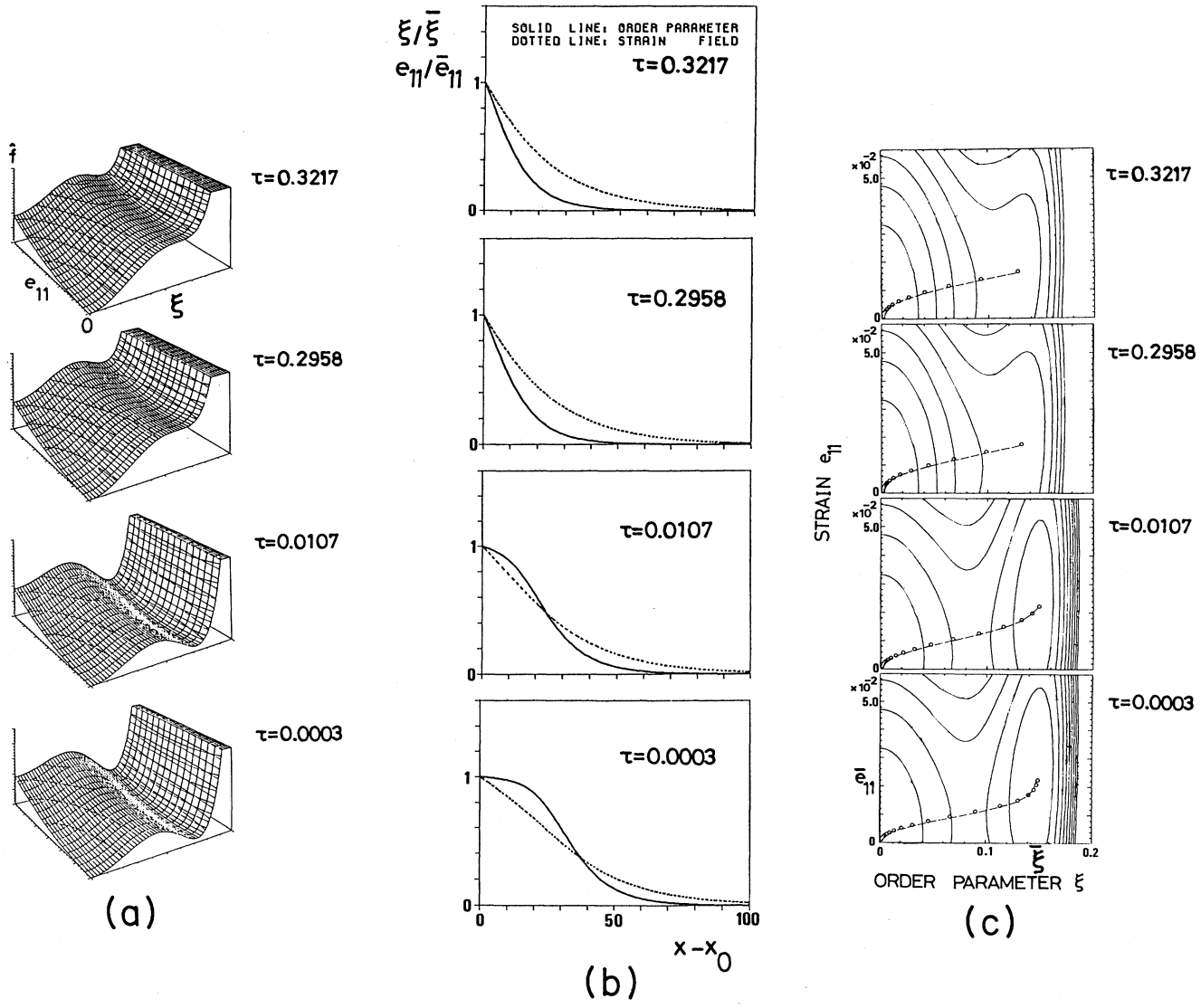

FIG. 3. (a) Potential surface within (ξ,e_{11}) space at various temperatures; from above, $\tau=0.3217$, $\tau=0.2958$, $\tau=0.0107$, and $\tau=0.0003$ ($\sim\tau_c$). (b) Spatial variations of ξ and e_{11} that are the solutions to Eq. (13) under the boundary condition (12) at the same temperatures as those in (a). Both ξ and e_{11} are normalized by $\bar{\xi}$ and $\bar{e}_{11}$, respectively. The embryo center x_0 is taken to be at origin. (c) Trajectories at those temperatures shown in (a) are plotted on the contour maps of the potential surfaces. Those shown by open circles are representative points plotted at equal interval Δx of the coordinate x. Note that these trajectories pass through the saddle point on the potential surface.

kink (soliton) boundary solution [Eq. (A2)] which separates a low-temperature embryo from the matrix phase.

It should be noted that the solution obtained in Eq. (16) has a somewhat unsatisfactory aspect in that $\partial\xi/\partial x \neq 0$ at $x = x_0$. Since we are assuming that $\xi(x) = \xi(-x)$, the above situation implies that the spatial derivative at $x = x_0$, $d\xi/dx|_{x=x_0}$ is discontinuous, which is not physically plausible. This point will be discussed in Sec. IV.

For the completeness of the discussion on the transformation, solutions to Eq. (14) with $\kappa_2 = 0$ for other temperature regions that are not concerned directly with the following discussion are shown in the Appendix A.

In case when κ_2 is included, it is impossible to solve Eq. (14) analytically. We have obtained numerically the solutions $\xi(x)$ and $e_{11}(x)$ following the iteration method developed by Ishibashi *et al.*[13] with a little improvement for effective convergence. Equations (16) and (18) were taken as initial configurations, and Eq. (14) was used to check whether or not the solutions were convergent. The calculated values of $\xi(x)$ and $e_{11}(x)$ for $\kappa_1 = 100$ and $\kappa_2 = 500$ are plotted in Fig. 3(b).

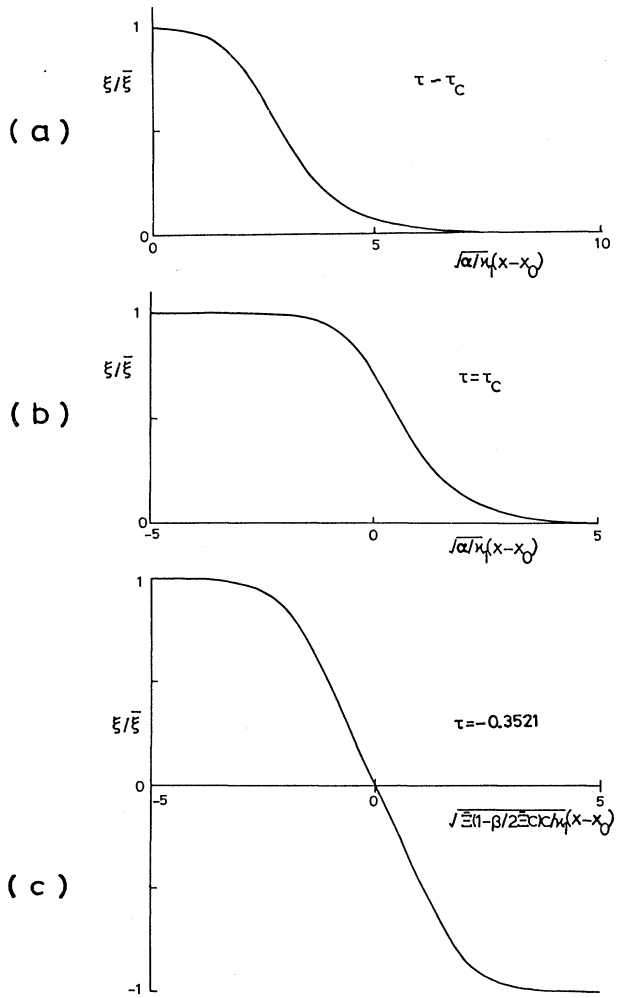

FIG. 4. Exact solutions to Eq. (14) for various temperatures when $\kappa_2 = 0$. x_0 is taken to be at origin. (a) An embryonic fluctuation [Eq. (16)] just above τ_c ($\tau = 0.0003$). (b) Antikink solution [Eq. (A2)] at the transition temperature. (c) Antikink solution [Eq. (A8)] below τ_c ($\tau = -0.3521$) representing the antiphase boundary separating two martensite variants.

The most interesting point of the numerical solutions is that as τ is decreased, the functional forms of $\xi(x)$ and $e_{11}(x)$ bear different characteristics; $\xi(x)$ becomes more kink (soliton) like, having interface region between the embryo and the mother matrix. (Previously, Yamada *et al.*[7-9] call the entity including the interface region a dressed embryo.) On the other hand, $e_{11}(x)$ simply shows gradual decay around $x = x_0$.

It is instructive to draw the trajectory within 2D ($\xi - e_{11}$) space by eliminating the spatial coordinate x from the solutions $\xi(x)$ and $e_{11}(x)$. This gives the lowest energy path from $(\bar{\xi}, \bar{e}_{11})$ to (0,0) to be followed by the representative point of the system as x is varied. The trajectories at various temperatures are included in Fig. 3(c). Notice that the representative points in the figure are plotted at an equal interval Δx of the coordinate x. Therefore, the density of the points along the trajectory directly reflects the length of persistence of the state in the real space. The high-density region around $(\bar{\xi}, \bar{e}_{11})$ corresponds to the embryonic fluctuation or the dressed embryo. In region (II), the total system should be expressed by random distribution of these embryonic fluctuations throughout the host lattice.

III. DIFFRACTION PATTERN

It is straightforward to obtain the diffraction pattern using the calculated values of $\xi(x)$ and $e_{11}(x)$ in the preceding section. Using Eq. (1), displacement of the nth atom associated with $\xi(x)$ is given by

$$\mathbf{u}_t(n) = \mathbf{e}(\mathbf{q}_0)\xi(n\mathbf{a})e^{i\mathbf{q}_0\cdot n\mathbf{a}} + \text{c.c.} \tag{19}$$

In addition, we have the longitudinal component due to the strain field $e_{11}(x)$,

$$\mathbf{u}_l(n) = \mathbf{e}_s e_{11}(n\mathbf{a}), \quad \mathbf{e}_s \| \mathbf{a} . \tag{20}$$

The diffraction spectrum $S(\mathbf{K})$ is obtained by

$$S(\mathbf{K}) = F(\mathbf{K})F^*(\mathbf{K}) , \tag{21}$$

$$F(\mathbf{K}) = \sum_n e^{i\mathbf{K}\cdot(n\mathbf{a}+\mathbf{u}_n)} , \tag{22}$$

$$\mathbf{u}_n = \mathbf{u}_t(n) + \mathbf{u}_l(n) . \tag{23}$$

In the calculation of the spectrum we neglect, for simplicity, the atomic scattering factor as well as the Debye-Waller factor. The calculated profiles of $S(hk0)$ ($k = 1$) are given in Fig. 5.

There are several important characteristics in the cal-

culated spectra.

(1) Throughout temperature range $0 \lesssim \tau < 0.3217$, the satellite peaks shift toward the origin of the reciprocal lattice, increasing the amount of shift as $|\mathbf{K}|$ is increased, while the fundamental Bragg peaks stay at the original regular positions. (See Fig. 6.)

(2) As the temperature is lowered below $\tau \lesssim 0.01$, the profile of the higher-order satellite peaks starts to show complicated structure. Particularly it tends to split into two peaks where the second peak seems to restore the commensurate positions.

(3) The Bragg peaks show appreciable tailing which is conventionally called Huang scattering[10] due to defects of various kinds.

The characteristic (1), of course, gives that of the ghost lattice or anomalous incommensurability. It is noticeable, however, that the satellite peak positions are approximately half way between the commensurate positions of the high-temperature and the low-temperature lattices which are on the two straight lines given in Fig. 6.

The physical origin of the ghost lattice is now clear; the strain field $e_{11}(x)$ around $x = x_0$ is essentially the same as those of a defect such as impurity, vacancy, etc. The resultant diffraction effect is Huang scattering around the Bragg peak which gives tailing but not shift of the peak positions. The embryonic fluctuation $\xi(x)$, on the other hand, gives rise to superlattice reflections. If there were no strain, the peak positions should be at the commensurate positions associated with the Bragg peaks. However, in the spatial region where $\xi(x) \neq 0$, the strain field has also appreciable finite values, which means that the embryonic fluctuations are preferentially embedded on the lattice with larger lattice constant; $a(1+\frac{1}{2}\bar{e}_{11})$ on average. Thus the satellite peak positions are at $\frac{1}{2}h(1-\frac{1}{2}\bar{e}_{11})a^*$ rather that at $\frac{1}{2}ha^*$.

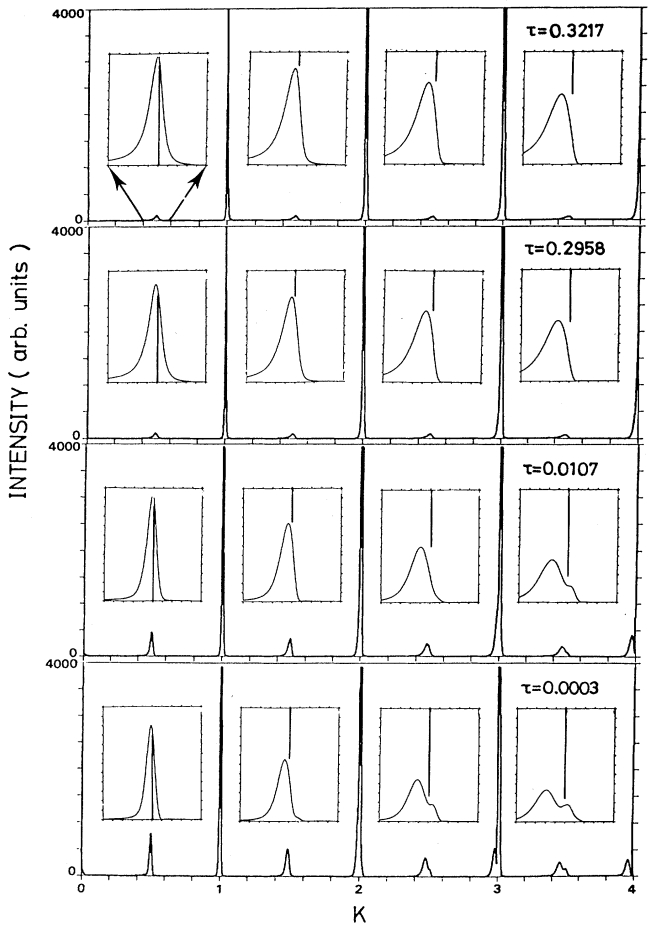

FIG. 5. Calculated diffraction patterns for $h \leq 4$, $k = 1$ at the same temperatures as those in Fig. 3. Notice the appreciable tailing (Huang scattering) of the fundamental Bragg peaks. The profiles of the satellites are shown in the insets with enlarged scales. The lines indicate the commensurate positions. It is apparent that superlattice reflections are shifted, with their amount of shift increasing as $|\mathbf{K}|$ is increased, toward the origin of the reciprocal lattice while the Bragg peaks center on the original reciprocal lattice points. Note that below $\tau \lesssim 0.01$ satellites split into two peaks where the second peak seems to restore the commensurate positions.

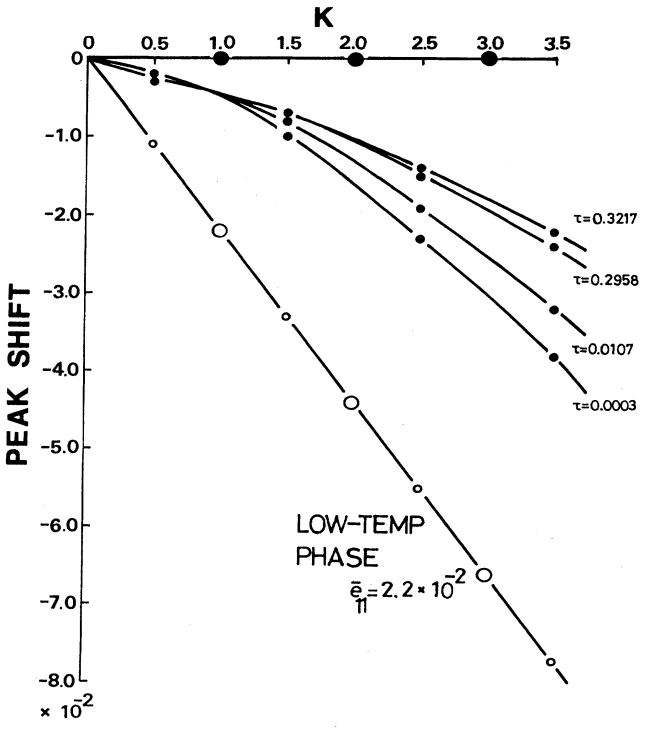

FIG. 6. Calculated ghost behavior of the superlattice reflections at $\tau > \tau_c$. Large solid circles represent the fundamental Bragg reflections and small solid circles represent the superlattice reflections. The fundamental reflections always stay at the original regular positions (on the horizontal line), while superlattice reflections tend to shift to the commensurate positions of the low-temperature lattice (shown by the open circles) as the temperature is lowered. Their actual positions are approximately half way between the commensurate positions of the high- and the low-temperature lattices.

IV. SUMMARY AND DISCUSSION

We have materialized, so to speak, the ghost by identifying that the origin of the anomalous incommensurability is due to embryonic fluctuation which is coupled strongly to the strain. The discussion is based on the general expression of free energy functional characterizing first-order phase transition. Therefore the results are not restricted by a microscopic lattice dynamical model as previously assumed in the case of β-based alloys. In principle, any crystal system undergoing first-order phase transition and satisfying the above condition (existence of strong coupling of order parameter to strain) would show ghost lattice behavior. More precise experimental investigations on various substances are certainly necessary.

As is described in Sec. III, one of the important characteristics of the calculated pattern is that the profile of higher-order satellites starts to split into two peaks as the temperature is lowered below $\tau \lesssim 0.01$. The secondary peaks are approximately on the commensurate positions. In the previous investigations on bcc metals NiTi(Fe)[4] and AuCd,[5] the satellites did show anomalous broadening but not splitting. Recently, however, Kiat *et al.*[14] observed definite splitting of satellites while fundamental Bragg peaks remain single peaks above the ferroelastic transition of $Pb_2(PO_4)_3$ crystal. This might be understood in terms of the characteristic feature described above.

Let us now discuss some problems still remaining in our treatment; the present treatment is based on the assumption that the system will be locally locked in at $\bar{\xi}=(\bar{\xi},\bar{e}_{11})$ by thermal activation. This point should be subjected to careful reinvestigation.

As is discussed in Appendix B, the solution of Eq. (14) (with $\kappa_2=0$) under the boundary condition of Eq. (12) seems to require the existence of a spatial singularity corresponding to the impulse at $x=x_0$ in the particle motion analogy. Physically, such spatial singularity may imply the presence of an impurity, defect, etc. at $x=x_0$. These considerations seem to be against our basic assumption that embryonic fluctuation is thermally excited in a homogeneous system without extrinsic heterogeneity such as impurity.

There is, however, another important possibility. The effect of impulse on $\xi(x)$ is manifested by the discontinuity of $d\xi/dx$ at $x=x_0$. The probable modification of the theoretical scheme to get rid of this singularity would be obtained by including higher-order derivatives such as $(\partial^2\xi/\partial x^2)^2$ in the free-energy density. That is, it would be necessary for describing correctly the immediate neighborhood of the embryo center to take shorter wavelength fluctuations into account. We conjecture that when this singularity is removed by including higher-order derivative terms, the embryonic fluctuations would be excited without any extrinsic heterogenity in the system.

Next we discuss the relation between our results for the 1D system and experimentally observed shift pattern of satellite reflections in 2D reciprocal space. Notice the results presented in Sec. III were calculated for the case in which $\lambda<0$. If we take $\lambda>0$ from the analogy to $\kappa_2=0$ case [Eq. (11)], then the longitudinal strain will be a contraction toward the embryo center, which results in a similar diffraction profile to those shown in Fig. 5 except that the direction of the shift is reversed. That is, all of the superlattice reflections shift away from the origin of the reciprocal lattice. If we extend the model to two-dimensional system in which λ is allowed to be orientation dependent in such a way that λ is negative in one direction and is positive in the other which is perpendicular to the former. This spatial dependence of the sign of λ may be expected to exist due to the intrinsic anisotropy of the parent structure. We can thus reproduce overall swirl shift pattern of superlattice reflections observed in NiTi(Fe)[4] and AuCd.[5]

ACKNOWLEDGMENTS

The authors are grateful to Dr. J. M. Kiat of Ecole Centrale de Paris for providing them with his experimental data prior to publication. Numerical calculations were made at Data Processing Center, Kyoto University.

APPENDIX A: EXACT SOLUTIONS OF EQ. (14) FOR OTHER TEMPERATURE REGIONS WHEN $\kappa_2=0$

We give here exact solutions to Eq. (14) when $\kappa_2=0$ for other temperature regions.

At T_c, $16\alpha c=3\beta^2$ holds. $\hat{f}(\xi,e_{11})$ then becomes

$$\hat{f}(\xi,e_{11})=(\sqrt{\alpha/2}\,\xi-\sqrt{c/6}\,\xi^3)^2 , \tag{A1}$$

which is now inserted to Eq. (14). Using the boundary condition $U_0=0$, Eq. (14) is readily integrated to give

$$\xi(x)=\pm\left[\frac{e^{\pm 2\sqrt{\alpha/\kappa_1}(x-x_0)}}{1+\frac{1}{\bar{\xi}^2}e^{\pm 2\sqrt{\alpha/\kappa_1}(x-x_0)}}\right]^{1/2} . \tag{A2}$$

If we take plus sign in front of the brackets, then $\xi(x)$ represents a phase boundary which separates from the matrix an embryo with the amplitude $\bar{\xi}$ at the embryo center, and if we take minus sign, $\xi(x)$ is a boundary separating an embryo of the other variant whose amplitude at the embryo center is equal to $-\bar{\xi}$. In the former if we take plus(minus) sign in the brackets, then the boundary is a (anti)kink [shown in Fig. 4(b) is the latter] while in the latter the results would be interchanged.

Below T_c [regions (III) and (IV)] the situation will change; we have to replace physically plausible boundary conditions as

$$\xi\to-\bar{\xi} \text{ as } x\to-\infty, \quad \xi\to\bar{\xi} \text{ as } x\to\infty$$

or (A3)

$$\xi\to\bar{\xi} \text{ as } x\to-\infty, \quad \xi\to-\bar{\xi} \text{ as } x\to\infty .$$

The corresponding U_0 to (A3) is

$$U_0=-\bar{U}=-\hat{f}(\bar{\xi},e_{11}(\bar{\xi}))\ .$$

Since

$$\hat{f}(\xi,e_{11})-\bar{U}=\frac{c}{6}(\Xi-\bar{\Xi})^2\left[\Xi+2\bar{\Xi}-\frac{3\beta}{2c}\right], \tag{A4}$$

where $\Xi=\xi^2$, $\bar{\Xi}=\bar{\xi}^2$, Eq. (14) becomes

$$\frac{1}{2}\frac{d\Xi}{\sqrt{c/6}\left[\left[\Xi+2\bar{\Xi}-\frac{3\beta}{2c}\right]\Xi(\Xi-\bar{\Xi})^2\right]^{1/2}}=\pm\sqrt{2/\kappa_1}dx\ . \tag{A5}$$

Using the elliptic integral of the first kind, Eq. (A5) is integrated to give

$$F(\phi,k=1)=\pm\left[\bar{\Xi}\left[\bar{\Xi}-\frac{\beta}{2c}\right]\frac{c}{\kappa_1}\right]^{1/2}(x-x_0)\ , \tag{A6}$$

$$\phi=\sin^{-1}\left[\frac{3\bar{\Xi}-\frac{3\beta}{2c}}{\bar{\Xi}}\frac{\Xi}{\Xi+2\bar{\Xi}-\frac{3\beta}{2c}}\right]^{1/2}\ .$$

Taking the inverse function,

$$\xi(x)=\pm\frac{\bar{\xi}\left[2-\frac{3\beta}{2\bar{\Xi}c}\right]^{1/2}\sinh\bar{\Xi}\left[\left[1-\frac{\beta}{2\bar{\Xi}c}\right]\frac{c}{\kappa_1}\right]^{1/2}(x-x_0)}{\left\{3-\frac{3\beta}{2\bar{\Xi}c}+\left[2-\frac{3\beta}{2\bar{\Xi}c}\right]\sinh^2\bar{\Xi}\left[\left[1-\frac{\beta}{2\bar{\Xi}c}\right]\frac{c}{\kappa_1}\right]^{1/2}(x-x_0)\right\}^{1/2}}\ , \tag{A8}$$

where $\xi(x)$ is a (anti)kink if the plus (minus) sign is chosen. In Eq. (A8) only the solution representing an antikink is shown in Fig. 4(c).

APPENDIX B: BOUNDARY CONDITIONS OF THE EULER EQUATION [EQ. (13)]

The problem to obtain the order parameter $\xi(x)$ around first-order phase transition was already discussed by Falk[15] in a simpler case (no coupling between the order parameter and some other quantities). He gave the solution in region (II) characterized by $\xi\sim\bar{\xi}$ as $x\to\pm\infty$ and $\xi\sim0$ at $x=0$. That is, a major part of the system takes the structure of the low-temperature phase, while only a small region around $x=0$ takes the structure close to the high-temperature phase [see Fig. 7(a)]. This result is qualitatively different from our solution given in Figs. 3(b) and 7(b).

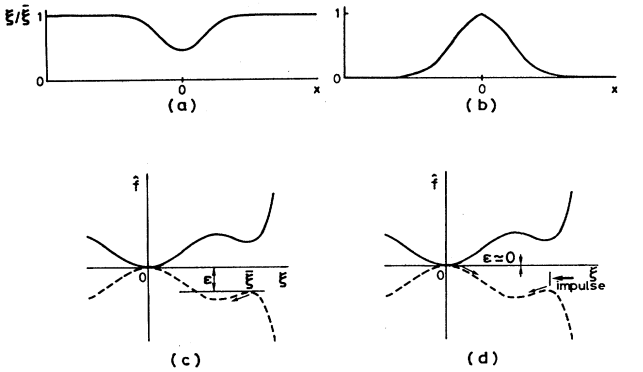

FIG. 7. (a) $\xi(x)$ in the temperature region (II) as obtained by Falk (Ref. 15). (b) Schematic picture of the embryonic fluctuation at $x=0$. Notice $d\xi/dx|_{x=0}$ has a singularity. (c) The particle motion analogy to the case of (a). A particle with mass κ_1 starts off at $\xi=\bar{\xi}$ with total energy ϵ within the potential $-\hat{f}$. (d) The particle motion analogy to the case of (b). A particle starts off at $\xi=0$ with total energy $\epsilon\simeq0$. An impulse is applied to bounce the particle back to $\xi=0$.

$$\phi=am\left[\pm\left[\bar{\Xi}\left[\bar{\Xi}-\frac{\beta}{2c}\right]\frac{c}{\kappa_1}\right]^{1/2}(x-x_0),\ k=1\right]$$
$$=\tan^{-1}\sinh\left\{\pm\bar{\Xi}\left[\left[1-\frac{\beta}{2\Xi c}\right]\frac{c}{\kappa_1}\right]^{1/2}(x-x_0)\right\}. \tag{A7}$$

Upon solving for Ξ and then taking a root, $\xi(x)$ can be obtained as

This is due to the different choice of the boundary conditions. In Falk's treatment, he imposed the following boundary conditions:

$$\partial\xi/\partial x=0\ \text{ at } x\to\pm\infty\ ,$$
$$\xi=\bar{\xi}\ \ [\hat{f}(\bar{\xi})=\epsilon]\ \text{ at } x\to\pm\infty \tag{B1}$$

with ϵ taking a finite positive value. This is different from the present boundary conditions given by Eq. (12). The physical meaning of this difference becomes clearer by noticing that when the coordinate x is replaced by time t, the Euler equation (13) (with $\kappa_2=0$) is equivalent to the equation of motion of a particle with mass κ_1 which is moving in the potential $(-\hat{f})$.

It is then easy to see that the solution given by Falk is equivalent to the motion of a particle which starts to move from $\xi=\bar{\xi}$ with total energy ϵ [see Fig. 7(c)]. The present solution corresponds to the following case: A

particle starts from $\xi=0$ with total energy $\epsilon\simeq 0$. As the particle reaches at $\xi=\bar{\xi}$, an impulse is applied to bounce back the particle to the opposite direction with exactly the same energy [Fig. 7(d)]. The former solution is physically improper to describe the precursor state because the total energy is linearly increasing with the system size, while the latter seems to imply that the system should have spatial singularities corresponding to the impulse.

[1]L. E. Tanner, A. R. Pelton, and R. Gronsky, J. Phys. (Paris) Colloq. **43**, C4-169 (1982); R. Oshima, M. Sugiyama, and F. E. Fujita, Met. Trans. **19A**, 803 (1988).

[2]M. B. Salamon, M. Meichle, C. M. Wayman, C. M. Huang, and S. M. Shapiro, in *Modulated Structures—1979 (Kailua Kona, Hawaii)*, Proceedings of the International Conference on Modulated Structures, AIP Conf. Proc. No. 53, edited by J. M. Cowley, J. B. Cohen, M. B. Salamon, and B. J. Buensch (AIP, New York, 1979), p. 223.

[3]G. Shirane and J. D. Axe, Phys. Rev. Lett. **27**, 1803 (1971); T. R. Finlayson and H. G. Smith, Met. Trans. **19A**, 185 (1988); M. Wuttig, C. Y. Lei, and T. Suzuki, *ibid.* **19A**, 789 (1988); A. Nagasawa, T. Makita, N. Nakanishi, M. Iizumi, and Y. Morii, *ibid.* **19A**, 793 (1988).

[4]S. M. Shapiro, Y. Noda, Y. Fujii, and Y. Yamada, Phys. Rev. B **30**, 4314 (1984).

[5]Y. Noda, M. Takimoto, T. Nakagawa, and Y. Yamada, Met. Trans. **19A**, 265 (1988).

[6]M. B. Salamon, M. E. Meichle, and C. M. Wayman, Phys. Rev. B **31**, 7306 (1985).

[7]Y. Yamada, Y. Noda, M. Takimoto, and K. Furukawa, J. Phys. Soc. Jpn. **54**, 2940 (1985).

[8]Y. Yamada, Y. Noda, and M. Takimoto, Solid State Commun. **55**, 1003 (1985).

[9]Y. Yamada, Met. Trans. **19A**, 777 (1988).

[10]P. H. Dederichs, J. Phys. F **3**, 471 (1973).

[11]This form of free-energy density can, in fact, be obtained from our semimacroscopic spin Hamiltonian (Ref. 12) that can describe generally the bcc (β)-martensite transformation by keeping the Fourier components of spin fluctuations up to $O(q^2)$.

[12]K. Fuchizaki, Y. Noda, and Y. Yamada, Phys. Rev. B **39**, 9260 (1989).

[13]Y. Ishibashi and V. Dvořák, J. Phys. Soc. Jpn. **44**, 32 (1978).

[14]J. M. Kiat (private communication).

[15]F. Falk, Z. Phys. B **51**, 177 (1983).